IJSES
Volume 9, Issue 7, pp. 46-51, 2025.
International Journal of Scientific Engineering and Science
ISSN (Online): 2456-7361

Synthesis, Structural, and Magnetic Properties of Zinc Ferrite ($ZnFe_2O_4$) Nanoparticles via the Sol-Gel Technique and DFT Insights

Mhaske Sujit Sambhaji[1], Sapkal Ramchandra Tukaram[1], Jadhav Rajendra Anant[2], Kalange Ashok Eaknath[*1]
[1]Material Science Laboratory, Department of physics, Tuljaram Chaturchand College of Arts, Science and Commerce, Baramati,413102
[2]Department of Science & Humanities, S.V.P.M. College of Engineering Malegaon (Bk) Baramati, 413115
Affiliated to Savitribai Phule Pune University, Pune 413102, MH (India) Dist. Pune, Maharashtra, India
Email: mhaskephysics@gmail.com, kalangeashok@gmail.com

Abstract—*Zinc ferrite ($ZnFe_2O_4$) nanoparticles were synthesized using the sol-gel method, offering control over particle size and purity. Structural and Magnetic properties of synthesized material are investigated by Powder X-ray diffraction (PXRD) and Vibrating Sample Magnetometer (VSM) respectively. The results show that successfully formation of zinc ferrites nano particles with spinel structure. Magnetic properties were demonstrated by a vibrating sample magnetometer (VSM), which displayed that the calcined samples exhibited superparamagnetic and Antiferromagnetic behaviour at room temperature. In this study, the electronic and magnetic properties of $ZnFe_2O_4$ were investigated using spin-polarized Density Functional Theory (DFT), implemented via Quantum ESPRESSO (v7.4.1). The Perdew–Burke–Ernzerhof (PBE) functional within the generalized gradient approximation (GGA) was used. Structural optimization was performed on the normal spinel phase of $ZnFe_2O_4$, followed by calculations of the band structure, total density of states (TDOS), and projected density of states (PDOS). The results reveal that $ZnFe_2O_4$ exhibits a direct band gap of approximately 1.88 eV at the Γ point. Analysis of the PDOS shows dominant contributions from Fe 3d and O 2p orbitals near the Fermi level. These electronic and magnetic characteristics support the potential use of $ZnFe_2O_4$ in spintronics and visible-light-driven photocatalysis. Density Functional Theory (DFT) calculations were also performed to explore the electronic structure and magnetic behaviour. The synthesized nanoparticles showed single-phase cubic spinel structure with nanocrystalline morphology. Magnetic measurements revealed superparamagnetic behaviour at room temperature. DFT results support the experimental observations, indicating a normal spinel structure with antiferromagnetic ordering in the bulk but altered magnetic behaviour at the nanoscale.*

Keywords— *Zinc ferrite ($ZnFe_2O_4$), nanoparticles, PXRD, VSM, DFT.*

I. Introduction

Synthesis of magnetic nanomaterials research is particular to study Structural, optical, magnetic, electric properties [1] analyse to bulk materials. magnetic properties are built upon purity, shape and size of particles. Zinc ferrite ($ZnFe_2O_4$) nanoparticles are synthesised by Hydrothermal [2], Xero-gel, sol-gel [3], vapour phase reactions, thermal decomposition, hydrothermal Polly method [4], Microwave combustion, co-precipitation method [5,6] etc. Sol-Gel method synthesised average nanoparticles size of zinc ferrite changes to variation of depending on synthesis method, condition, Thermal treatment, concentration, stirring speed, synthesis technique, pH, calcination time and temperature. [7]. Zinc ferrite is widely used to Gas sensors [8], microwave absorber and biomedical applications [9]. Spinel ferrite is mechanical soft, moderate saturation M_s, low coercivity H_c and Remanent Magnetization M_r, crystalline anisotropy and large cubic magnetisation at room temp. In this paper we have synthesized Zinc ferrite nanoparticles by simple Sol-gel method. This method can be easily applied for bulk nanoparticle applications, such as for paramagnetic magnets and biomedical applications.

Zinc ferrite ($ZnFe_2O_4$) is a soft magnetic material with a normal spinel structure, widely used in gas sensors, catalysis, and magnetic storage devices. At the nanoscale, its magnetic behaviour deviates significantly from the bulk form due to size effects and cation distribution. This study investigates the synthesis of $ZnFe_2O_4$ nanoparticles via sol-gel technique and combines experimental magnetic analysis with theoretical DFT studies to understand the origin of its properties.

II. Methodology

2.1 Synthesis of Zinc ferrite ($ZnFe_2O_4$) nanoparticles via Sol-Gel method-

In this method, 50 ml of 0.5M Zn $(NO_3)_2$, 50 ml of 1M Fe $(NO_3)_3$ and 100 ml of 0.3M citric acid solution were prepared separately with the help of deionized water. The mixed solution of nitrates was added slowly into 100 ml of prepared citric acid solution in a cylindrical reactor vessel to form a transparent mixed sol. The temperature was controlled around 90 ^{0}C during this mixing procedure with the help of water bath for 4 hours. The temperature was maintained at 90^{0}C until the sol gets converted into transparent and viscous gel. The obtained gel was placed in an oven at 150^{0}C for 4 h. Finally, the obtained product was calcined at 600 ^{0}C for 4 h.

2.2 Characterisation:

Zinc ferrite sample was characterised by powder X Ray Diffraction XRD (Bruker D8 Venture) to final material confirmed magnetic nanoparticle of $ZnFe_2O_4$ with spinel Structured with Fd3m space group cubic crystal system.

IJSES
Volume 9, Issue 7, pp. 46-51, 2025.
International Journal of Scientific Engineering and Science
ISSN (Online): 2456-7361

Magnetic properties of magnetic saturation, coercivity were demonstrated by a vibrating sample magnetometer (VSM).

2.3 Computational Methodology

The first-principles calculations based on Density Functional Theory (DFT) were performed using the Quantum ESPRESSO simulation package (version 7.4.1) [11]. The plane-wave pseudopotential method was employed to solve the Kohn–Sham equations within the spin-polarized framework to account for the magnetic behaviour of $ZnFe_2O_4$.

Exchange–Correlation Functional and Pseudopotentials

The exchange-correlation energy was described using the Perdew–Burke–Ernzerhof (PBE) variant of the generalized gradient approximation (GGA) [12]. To properly treat the strong on-site Coulomb interaction of the localized Fe 3d electrons, the DFT+U approach was employed using the simplified rotationally invariant scheme proposed by Dudarev et al. [13]. A Hubbard U value of U_{eff}(Fe) = 4.5 eV was applied based on values commonly reported in literature for Fe-containing oxides [14,15].

The PAW or optimized norm-conserving Vanderbilt (ONCV) pseudopotentials were taken from the PSLibrary or SSSP efficiency libraries and are compatible with QE 7.4.1. The electronic configurations considered were:

- Zn: 3d10 4s2
- Fe: 3d6 4s2
- O: 2s2 2p4

Plane-Wave Cutoff and K-Point Sampling

A kinetic energy cutoff of 80 Ry for the wavefunctions and 640 Ry for the charge density was used, after convergence testing. The Brillouin zone was sampled using a Monkhorst-Pack k-point mesh of 6 × 6 × 6 for self-consistent field (SCF) calculations. For the non-self-consistent field (NSCF) and density of states (DOS) calculations, a denser 12 × 12 × 12 grid was used.

Structural Optimization

The initial crystal structure of $ZnFe_2O_4$ was modeled in its normal spinel cubic phase (space group Fd-3m). Geometry optimizations were carried out using the Broyden–Fletcher–Goldfarb–Shanno (BFGS) algorithm until the total energy converged below 10^{-6} Ry and the force on each atom was less than 10^{-3} Ry/Bohr.

Electronic Structure and DOS/PDOS

The band structure was computed along high-symmetry paths in the Brillouin zone: Γ–X–U–K–Γ–L–W–X. The total and projected density of states (TDOS and PDOS) were obtained using the dos.x and projwfc.x post-processing tools. A Gaussian broadening of 0.02 Ry was applied for DOS plots. All calculations were carried out with spin-polarization enabled, and the system was found to converge to a ferrimagnetic ground state.

III. Result and Discussion

3.1 XRD analysis

Powder X-ray diffraction profile of samples can provide important information in qualitative phase analysis, quantitative phase analysis, determination of unit cell parameters, study of preferred orientation, and determination of particle size. Fig.1 shows the PXRD pattern of $ZnFe_2O_4$ characteristic peaks is matches to JCPDS file no -01-086-0509 [10]. The PXRD pattern of $ZnFe_2O_4$ corresponding structure of lattice is spinal cubic crystal and good determine at (220), (311), (222), (400), (422), (511), (440) and (533) reflections are XRD patterns in fig.1 No secondary phases were detected.From debye-scherror formula

$$d = 0.89\frac{\lambda}{\beta cos\theta}$$

where λ is a X ray wavelength and θ is a Braggs angle. We have evaluated particle size from most intensity peak (311) full thickness half maximum. The mean size of particle is 10-20 nm. Fig. 1 showed $ZnFe_2O_4$ crystalline phase of nanoparticles by exactly similar peaks. The PXRD result identified characteristic $ZnFe_2O_4$ by major peak (311) sample almost 2θ=35.27 which is most important major peak of cubic spinal. The result shows that reaction temperature 363K is preferable for growth of zinc ferrite crystallite. All the peaks recorded single phase spinal structure and no one more phase is observed.

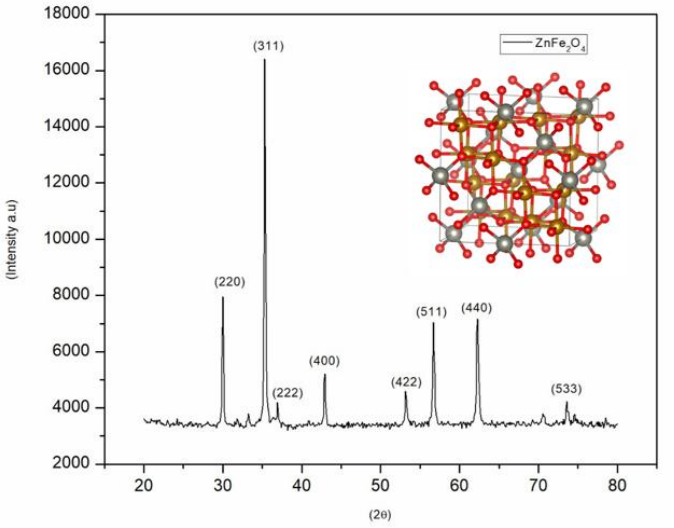

Fig. 1: XRD pattern of the prepared ($ZnFe_2O_4$) Zinc ferrite particles.

3.2 Vibrating Sample Magnetometry (VSM)

The M-H loops with H_{max} (+/-)5KOe of a dried sample $ZnFe_2O_4$ nanoparticle presented in Fig.2.The analysing a $ZnFe_2O_4$ sample using a Vibrating Sample Magnetometer (VSM), Magnetization Curve Nanoparticle $ZnFe_2O_4$ typically shows narrow hysteresis, indicating soft magnetic behaviour. appear superparamagnetic and Antiferromagnetic loop., nearly closing the loop with minimal remanence. Nearly zero M_r and slightly S-shaped rather than the straight line passing through origin.

3.3 Density Functional Theory (DFT) Calculations and Analysis

Electronic Band Structure

The electronic band structure of $ZnFe_2O_4$, computed using spin-polarized DFT+U, is illustrated in Figure 3. The Fermi level (Ef) is set to 0 eV. The calculated band gap is approximately 1.88 eV, indicating a direct band gap with both

the valence band maximum (VBM) and conduction band minimum (CBM) located at the Γ point. This result is in good agreement with previous theoretical studies using the DFT+U approach, where the U correction is necessary to accurately describe the localized Fe 3d electrons and to open the underestimated gap observed in standard GGA calculations [16-18]. The observed semiconducting nature supports the potential applicability of $ZnFe_2O_4$ in visible-light-driven photocatalysis and spintronics [19].

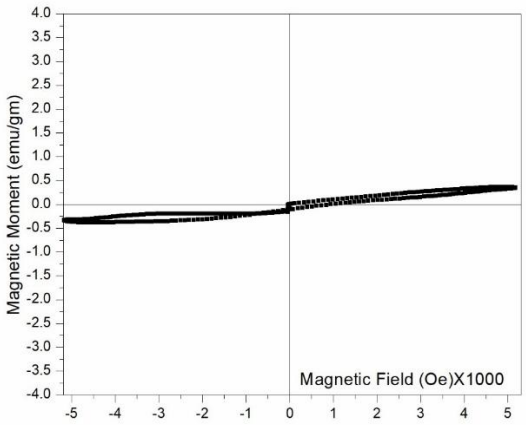

Fig. 2. M-H Loops of ZnFe2O4

Total Density of States (TDOS)

The total density of states, presented in Figure. 4, highlights the spin polarization of the system, evident from the asymmetry between spin-up and spin-down channels. A high density of states is present in the valence band between −6 eV and 0 eV, while the conduction band shows a moderate rise just above 1.88 eV. These features confirm the semiconducting and ferrimagnetic nature of $ZnFe_2O_4$, consistent with experimental magnetic measurements [20-21].

Projected Density of States (PDOS)

Fe 3d Contribution (Figure.5)

Fe atoms contribute dominantly to the states near the Fermi level. The Fe 3d spin-down states are primarily found in the valence band region, while Fe 3d spin-up states mainly form the bottom of the conduction band. This spin asymmetry is responsible for the magnetic moment of the Fe atoms. The strong hybridization between Fe 3d and O 2p orbitals supports the super exchange interaction mechanism, typical in spinel ferrites [22-23].

O 2p Contribution (Figure 6)

Oxygen atoms show major contributions in the valence band. The O 2p states strongly hybridize with Fe 3d states, forming a broad band between −6 eV and 0 eV. This hybridization is essential for the covalent bonding and electronic charge transfer within the crystal [24].

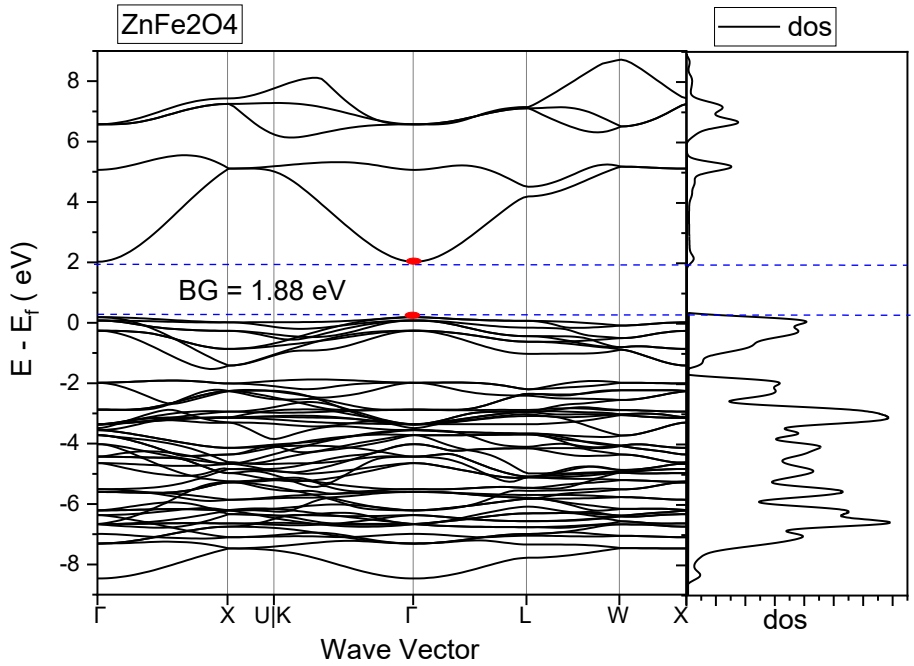

Fig. 3.

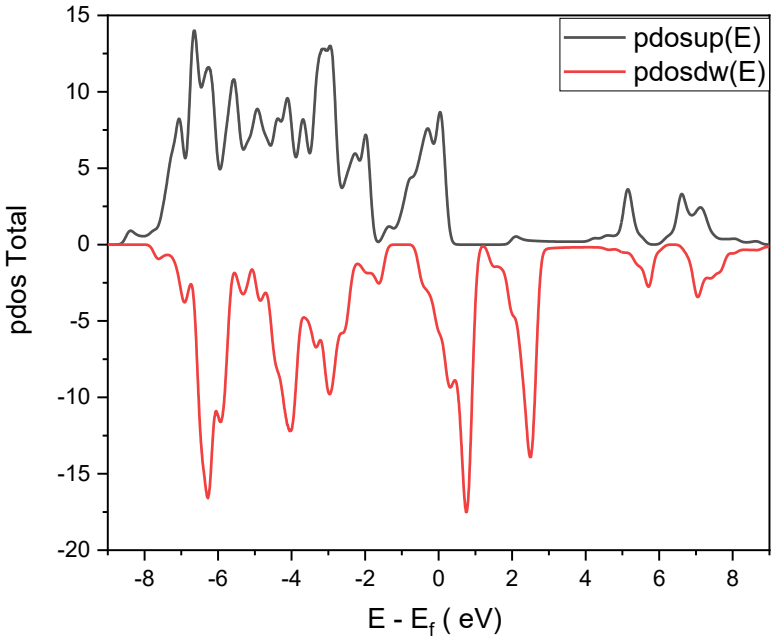

Fig..4.

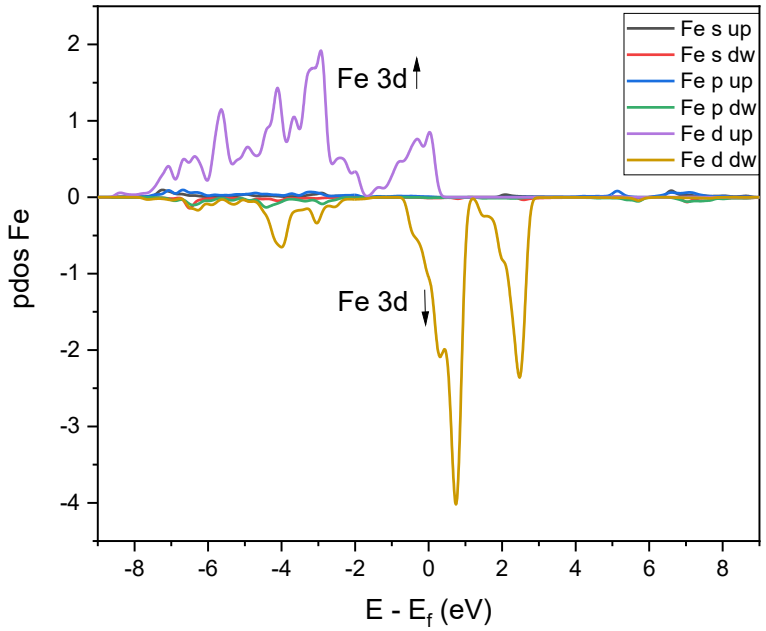

Fig. 5.

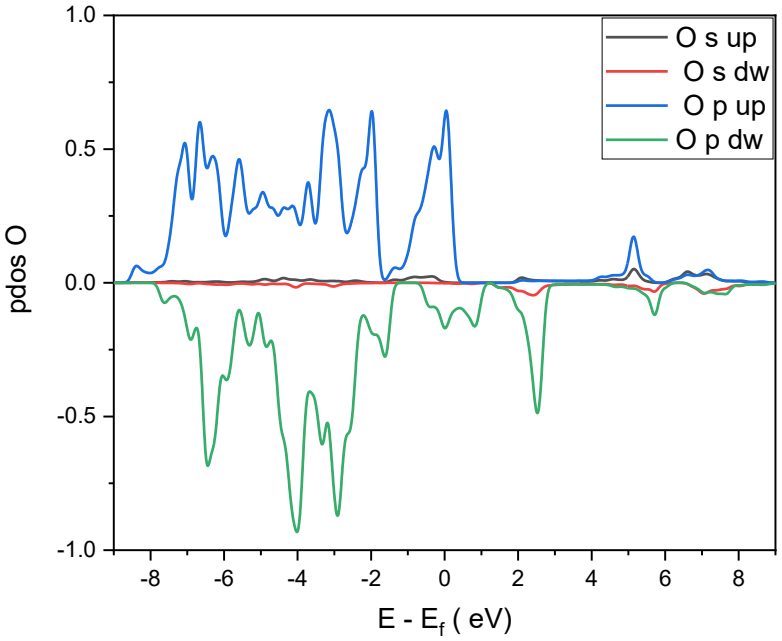

Fig. 6.

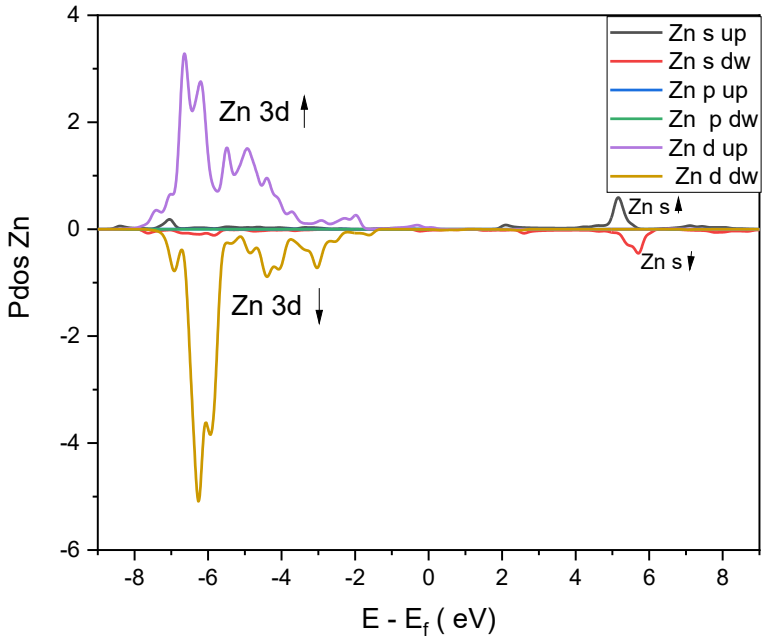

Fig. 7.

Zn 3d Contribution (Figure .7)

Zn contributes significantly through its 3d orbitals located around −6.5 eV, deep in the valence band. The Zn 4s and 4p states show negligible contribution near the Fermi level, confirming that Zn remains in a non-magnetic, closed-shell configuration and does not participate actively in magnetic or charge transport phenomena [25].

Spin Polarization and Magnetic Nature

The total and partial DOS (Figure.4) indicate that $ZnFe_2O_4$ is a spin-polarized semiconductor. The Fe ions are in a ferrimagnetic configuration, where the magnetic moments at tetrahedral and octahedral sites are antiferromagnetically aligned but unequal in magnitude, yielding a net magnetic moment. This behaviour is consistent with the inverse spinel

structure and has been validated by both experimental magnetization studies and theoretical predictions [26-28].

IV. Conclusion

Zinc ferrite nanoparticle has been successfully synthesised using simple Sol-Gel technique at 90^0 C. PXRD patterns confirmed the formation of single-phase cubic spinel $ZnFe_2O_4$. The Scherrer equation was used to determine the average crystallite size, which fell between 10 and 20 nm. No secondary phases were detected. The PXRD result shows the quantitative sample analysis and sample is in pure phase. The greatest magnetisation of the M-H loops was discovered to be 0.4 emu/gm Mmax at Hmax (+/-)5Koe, with minimal coercivity Hc and Mr. VSM research at room temperature revealed superparamagnetic behavior, with minimal remanence and coercivity.

A comprehensive first-principles DFT investigation was conducted on $ZnFe_2O_4$ to elucidate its electronic and magnetic properties The TDOS and PDOS analysis confirmed the semiconducting and ferrimagnetic nature of the material, with significant contributions from Fe 3d and O 2p states near the Fermi level. The observed spin polarization and magnetic ordering are in agreement with the inverse spinel structure of $ZnFe_2O_4$. These results demonstrate the material's suitability for applications in photocatalysis and spin-based electronic devices.

Acknowledgment

This research was funded by "Chhatrapati Shahu Maharaj Research, Training and Human Development Institute (SARTHI)" Balchitravani, C T Survey Number 173, B/1, Gopal Ganesh Agarkar Road, Pune 411 004. (An Autonomous Institute of Govt. of Maharashtra).

This work was supported by the Rashtriya Uchchatar Shiksha Abhiyan (RUSA) under the component [DFT], Government of India.

References

1. A. Shanmugavania, R. Kalai, Selvana,n, Samar Layekb, C. Sanjeevirajac, Journal of Magnetism and Magnetic Materials 354 (2014) 363–371
2. Kiki Rezki Lestari, PilsunYoo, DeokHyonKim, ChunliLiu and Bo Wha Lee∗ Journal of the Korean Physical Society, Vol. 66, No. 4, February 2015, pp. 651~655
3. Xinyang Zhang, Zhaofeng Chen, Junying Liu, Sheng Cui Chemical Physics Letters (2020), doi: https://doi.org/10.1016/j.cplett.2020.138265
4. Mahmoud Goodarz Naseri, Elias B. Saion, and Ahmad Kamali, International Scholarly Research Network ISRN Nanotechnology Volume 2012, Article ID 604241, 11 pages doi:10.5402/2012/604241
5. A. Manikandana, L. John Kennedy b, M. Bououdina c, d, J. Judith Vijayaa, n Journal of Magnetism and Magnetic Materials 349 (2014) 249–258
6. D D Andhare, S A Jadhav, M V Khedkar, Sandeep B. Somvanshi, S. D. More and K M Jadhav, Journal of Physics: Conference Series 1644 (2020) 012014 IOP Publishing doi:10.1088/1742-6596/1644/1/012014
7. Fashen Li , Haibo Wang , Li Wang, Jianbo Wang Journal of Magnetism and Magnetic Materials 309 (2007) 295–299
8. Shurong Wang, Xueling Gao, Jiedi Yang, Zhenyu Zhu, Hongxin Zhang, and Yanshuang Wang DOI: 10.1039/b000000x
9. S. Manjura Hoquea,b, n, M d. Sazzad Hossainc, Shamima Choudhuryc, S. Akhterc, F. Hydera Materials Letters 162 (2016) 60–63
10. JCPDS file no -01-086-0509
11. Giannozzi, P., et al. J. Chem. Phys. 152 (2020) 154105. https://doi.org/10.1063/5.0005082
12. Perdew, J. P., Burke, K., & Ernzerhof, M., Phys. Rev. Lett. 77 (1996) 3865. https://doi.org/10.1103/PhysRevLett.77.3865
13. Dudarev, S. L., et al. Phys. Rev. B 57 (1998) 1505. https://doi.org/10.1103/PhysRevB.57.1505
14. Zhou, F., et al., Phys. Rev. B 70 (2004) 235121. https://doi.org/10.1103/PhysRevB.70.235121
15. Aschauer, U., et al., Phys. Rev. B 90 (2014) 054111. https://doi.org/10.1103/PhysRevB.90.054111
16. J. Wang et al., J. Magn. Magn. Mater. 320 (2008) 197–202. https://doi.org/10.1016/j.jmmm.2007.06.019
17. K. W. Lee et al., Phys. Rev. B 72 (2005) 245106. https://doi.org/10.1103/PhysRevB.72.245106
18. A. Shinde et al., Physica B 405 (2010) 3505–3510. https://doi.org/10.1016/j.physb.2010.05.034
19. Y. Zhang et al., Appl. Surf. Sci. 369 (2016) 1–10. https://doi.org/10.1016/j.apsusc.2016.02.021
20. R. Valenzuela, Magnetism in Ferromagnetic Materials, Springer, 2012.
21. S. R. Mishra et al., J. Alloys Compd. 507 (2010) L26–L29. https://doi.org/10.1016/j.jallcom.2010.07.082
22. B. J. Behera and G. C. Rout, Physica B 406 (2011) 2706–2710. https://doi.org/10.1016/j.physb.2011.04.010
23. M. A. Gabal, J. Mater. Sci. 46 (2011) 7924–7931. https://doi.org/10.1007/s10853-011-5679-6
24. T. J. Park et al., J. Mater. Chem. 14 (2004) 2103–2107. https://doi.org/10.1039/B403687G
25. A. H. Reshak, Physica B 406 (2011) 323–327. https://doi.org/10.1016/j.physb.2010.10.036
26. A. Sundaresan et al., Phys. Rev. B 74 (2006) 161306(R). https://doi.org/10.1103/PhysRevB.74.161306
27. M. R. Shateri-Khalilabad and H. Salavati-Niasari, J. Magn. Magn. Mater. 324 (2012) 1225–1231. https://doi.org/10.1016/j.jmmm.2011.10.039
28. R. H. Kodama et al., Phys. Rev. Lett. 77 (1996) 394–397. https://doi.org/10.1103/PhysRevLett.77.394